J Mater Sci (2010) 45:6593–6598
DOI 10.1007/s10853-010-4748-1

Crystallization kinetics of an amorphous $Al_{75}Ni_{10}Ti_{10}Zr_5$ alloy

Xiu Wei · Xingfu Wang · Xinfu Wang · Fusheng Han

Received: 7 February 2010 / Accepted: 1 July 2010 / Published online: 17 July 2010
© Springer Science+Business Media, LLC 2010

Abstract The formation and crystallization behaviors of a mechanically alloyed $Al_{75}Ni_{10}Ti_{10}Zr_5$ amorphous alloy were studied by X-ray diffraction, transmission electron microscopy, and differential scanning calorimetry in the present study. The effective activation energy of the crystallization was determined by the Kissinger and Ozawa equations, respectively. The two equations yield close results and the average activation energy is 252 ± 13 kJ/mol. The resultant crystalline products were Al and Al_3Ni, and the crystallization mechanism is two- or three-dimensional nucleation and growth controlled by the diffusion of atoms. The thermal stability of the alloy was evaluated by a continuous transformation diagram obtained by the extended Kissinger equation.

Introduction

Al-based amorphous alloys have attracted much attention in recent years due to their low densities and high mechanical properties, which makes them prospective candidates in light-weight structures in aerospace and other engineering fields [1]. Compared with other conventional metallic glasses, the Al-based alloys have relatively weak glass-forming abilities that do not obey the general atomic size criteria [2, 3]. It is very difficult for Al-based or Al-rich alloys to form amorphous structure. The maximum amorphous material thickness available through rapid solidification is less than 1 mm up to date, limiting their applications in engineering fields. In addition to rapid solidification, mechanical alloying is another very effective technology to make amorphous alloys particularly for those systems with insufficient glass forming ability [4–8]. Based on the mechanically alloyed amorphous powders, the bulk glasses can be produced via a powder metallurgy route such as consolidation and equal channel angular extrusion in the supercooled liquid region. This makes it possible to produce bulk metallic glasses in more extensive ranges of size and shape [9, 10].

The thermal stability of amorphous powders during consolidation and subsequent cooling is extremely important for obtaining fully amorphous structure in the resultant bulk materials, which can be realized by optimizing the chemical composition and mechanical alloying process. Nevertheless, although monolithic amorphous structure gives metallic glasses unique mechanical properties, and particularly very high ratio of strength to elastic modulus, they show almost no macroscopic plastic strain, limiting their usefulness as structural materials. In order to overcome this shortage, many methods have been developed, such as precipitation of nano-crystalline phase or formation of porosity in the materials, in which the appearance of nano-crystalline grains in an amorphous matrix is believed to be able to obstruct the propagation of shear-band and thus significantly improve the ductility of the alloys [11–15]. The nano-crystalline grains can be formed via crystallization heat treatment of bulk amorphous alloys. In this circumstance, it is essential to understand the thermal stability and crystallization kinetics of an amorphous alloy.

In the present work, an $Al_{75}Ni_{10}Ti_{10}Zr_5$ amorphous alloy was synthesized by mechanical alloying process that shows relatively high crystallization temperature and wide supercooled liquid region. The long-term thermal stability and non-isothermal crystallization kinetics of the alloy were investigated to give fundamentals for the proceeded consolidation and crystallization processes.

X. Wei · X. Wang · X. Wang · F. Han (✉)
Key Laboratory of Materials Physics, Institute of Solid State Physics, Chinese Academy of Sciences, Hefei 230031, China
e-mail: fshan@issp.ac.cn

Experimental

Elemental pure metal powders (99.9% purity) of Al, Ni, Ti, and Zr were used and weighted according to the nominal composition (at.%) of 75Al, 10Ni, 10Ti, and 5Zr. The mechanical alloying (MA) process was conducted in a planetary ball mill (QM-3SP4L) operated at 400 rpm using stainless steel vial and bearing balls with a ball to powder weight ratio of 20:1 in an argon atmosphere. When the pot rotated, cold air was blown over it to avoid elevated temperatures. The milling process was stopped at given times to take out powder samples from the pot for analysis. The operation of powders was performed in a glove box with a pure argon gas environment to minimize contamination. The phases and structures of milled powders were characterized by X-ray diffraction (XRD) using Cu Kα radiation (X'Pert Pro MPD), and transmission electron microscopy (TEM, JEOL 2010), respectively. The samples for TEM observation were dispersed into a pure ethanol solution first, and then oscillated in a supersonic apparatus for 10 min before dropping onto a copper mesh coated with carbon film. The thermal stability and crystallization kinetics of the powders were evaluated by differential scanning calorimetry (DSC, Pyris Diamond) at different heating rates under nitrogen atmosphere.

Results and discussion

Figure 1 shows the XRD patterns of $Al_{75}Ni_{10}Ti_{10}Zr_5$ powders after different milling times. It is evident that the characteristic peaks of the constituent elements gradually decreased in intensity and increased in width. After 110 h milling, all the diffraction peaks typical for crystalline phases disappeared and a broad diffraction peak appeared, demonstrating the formation of a fully amorphous structure. This weakening process of the peaks actually reflects a dissolution process occurred among the elements, whilst the broadening of the peaks suggests a decreased effective grain size and/or an increased strain within the grains. The dissolution started with Ni dissolving in Al to form Al–Ni solid solution and intermetallic compounds, continued with Ti dissolving in Al–Ni solid solution, and ended by Zr dissolving in Al–Ni–Ti solid solution [16, 17].

To confirm the phase nature of powder milled for 110 h, the microstructures were examined under TEM, as shown in Fig. 2. It is seen that the powder shows a very fine and homogeneous microstructure, and a diffusive halo typical for amorphous structures, being in agreement with the XRD pattern shown in Fig. 1.

The featured temperatures of the amorphous powder were measured by DSC at varied heating rates. It is seen from Fig. 3 that for the powder milled for 110 h, the onset

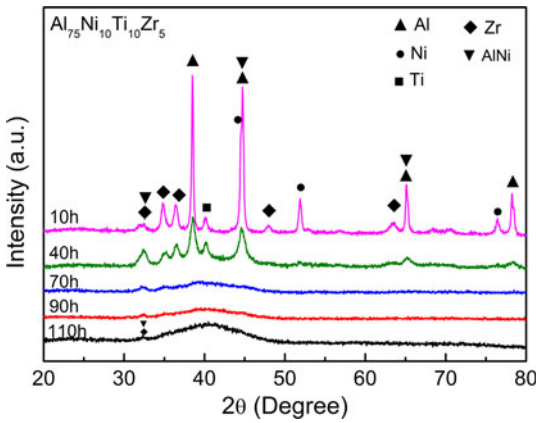

Fig. 1 XRD patterns of the $Al_{75}Ni_{10}Ti_{10}Zr_5$ alloy milled for varied times

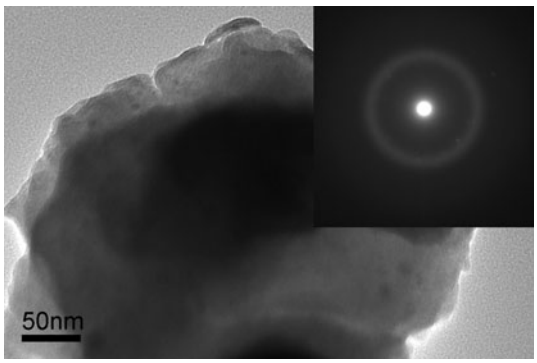

Fig. 2 TEM bright-field image and selected area diffraction pattern of $Al_{75}Ni_{10}Ti_{10}Zr_5$ powder milled for 110 h

crystallization temperature (T_x^{onset}) and peak crystallization temperature (T_x^{peak}) were delayed to higher temperatures. The supercooled liquid region $\Delta T_x = T_x^{onset} - T_g$ (where T_g is the onset temperature of glass transition [18]) is 49 K at the heating rate of 20 K/min. In order to determine the crystallized structures of the powder, the sample milled for 110 h was annealed at 798 K for 2 h and then characterized by XRD. As shown in Fig. 4, the crystallized products are Al and Al_3Ni.

Using the heat flow (Φ)–temperature (T) data of DSC measurements at different heating rates, the crystallization fraction (X)–T plots can be obtained, as shown in Fig. 5. The curves have a typical sigmoid feature and the inoculation time of crystallization increased with increasing heating rates. For a given heating rate, the crystallization rate was relatively slow at both the beginning and the end, while it was very quick when the crystallization fraction was between 20 and 80%. At the initial stage, the nucleation rate is low due to the low diffusion of atoms at low temperature. Therefore, the crystallization rate is slow. As the temperature increases, external energy overcomes

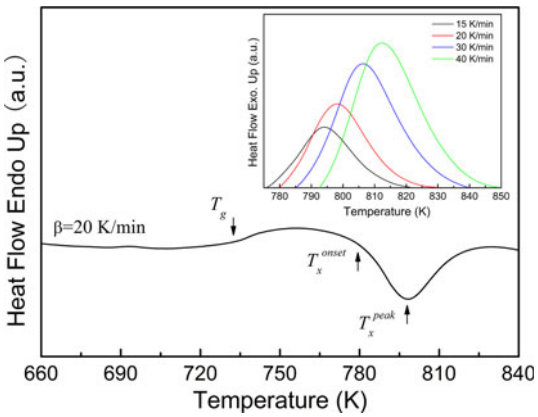

Fig. 3 DSC curves of $Al_{75}Ni_{10}Ti_{10}Zr_5$ amorphous alloy at different heating rates

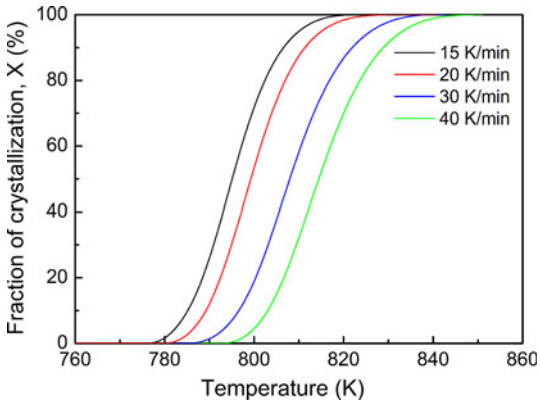

Fig. 5 Crystallization volume fraction as a function of temperature

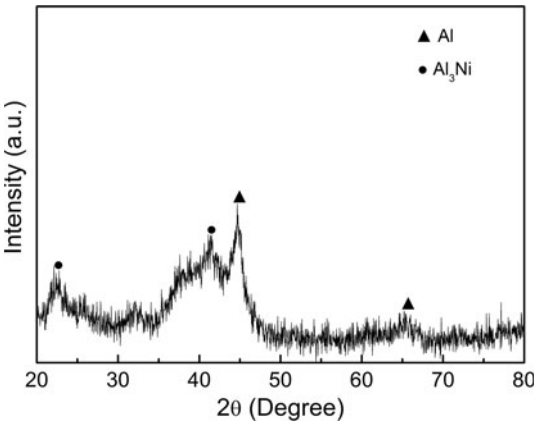

Fig. 4 XRD pattern of $Al_{75}Ni_{10}Ti_{10}Zr_5$ amorphous alloy annealed at 798 K for 2 h

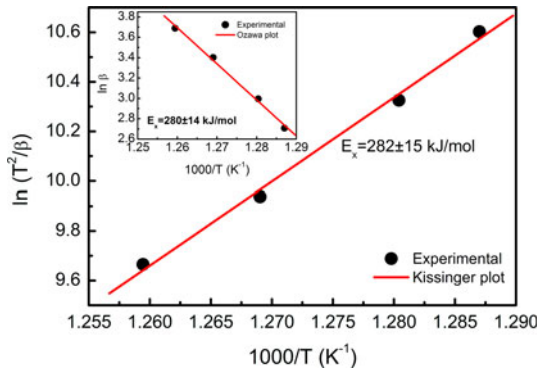

Fig. 6 Kissinger and Ozawa plots for the $Al_{75}Ni_{10}Ti_{10}Zr_5$ amorphous alloy at varied peak crystallization temperatures

the nucleation barrier, and large numbers of nuclei form, which hastens the crystallization process. At the final stage, the rate of crystallization slows down again due to the decrease of the number of the preferential nucleation sites.

The effective activation energy, E_a, for the observed peak temperatures at varied heating rates can be determined by Kissinger or Ozawa equation [19, 20], that is

$$\ln(T^2/\beta) = E_a/RT + c_1 = E_a/RT + \ln(E_a/RK_0), \quad (1)$$

$$\ln\beta = -AE_a/RT + c_2, \quad (2)$$

where β is the heating rate, R the gas constant, T the peak temperature, A a constant and equals 1.0516, c_1 and c_2 constants, and K_0 the frequency factor in Arrhenius equation. As is seen in Fig. 6, Ozawa and Kissinger curves are approximately straight lines, suggesting that only one reaction mechanism is operative in this range of heating rates. Table 1 lists T_x^{onset} and T_x^{peak} at different β values as well as the effective activation energies calculated by Kissinger (E_{ak}) and Ozawa (E_{ao}) equation, respectively. Obviously, the two equations yield almost the same effective energy. The estimated activation energy from the onset crystallization temperature is about 282 ± 15 kJ/mol. It is higher than those observed in Al–TM–TM (TM: transition metals) amorphous alloys by other researchers [21–24], suggesting that the present $Al_{75}Ni_{10}Ti_{10}Zr_5$ amorphous alloy is more stable. The frequency factor K_0, usually written as the product of atom collision probability and steric factor, is a measure of the probability that an atom having energy E_a participates during the crystallization. By collision, some atoms will acquire additional energy or activation energy to join or to be part of activated clusters [25, 26]. Obviously, the collision probability of atoms at the early stage of crystallization is much greater than that at the peak temperature, and thus the crystallization rates are much higher at this stage, too.

The local activation energy of crystallization, which reflects the changes in the nucleation and growth rates during the crystallization process, can be determined by Flynn–Wall–Ozawa (FWO) relation [27], that is

$$\ln\beta = -AE_a(x)/RT(x) + C_2, \quad (3)$$

Table 1 Characteristic temperatures and kinetic parameters for the $Al_{75}Ni_{10}Ti_{10}Zr_5$ amorphous alloy determined by non-isothermal analysis

	β (K/min)				E_{ak} (kJ/mol)	E_{ao} (kJ/mol)	K_0 (min^{-1})
	15	20	30	40			
T_x^{onset} (K)	777	781	788	794	281.5	280.1	1.9×10^{20}
T_x^{peak} (K)	794	798	806	812	274.0	273.3	8.6×10^{18}

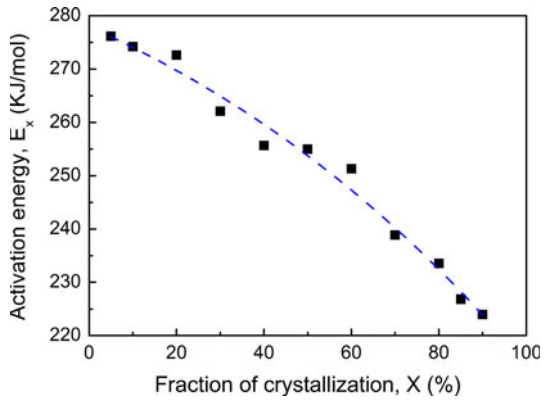

Fig. 7 Variation of the local activation energy with the crystallization volume fraction derived from the FWO equation

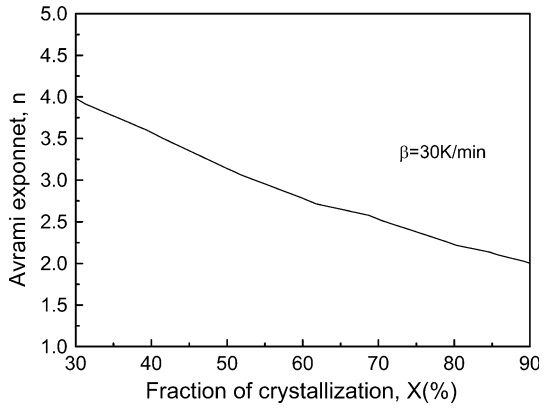

Fig. 8 The Avrami exponent as a function of crystallized volume fraction at a heating rate of 30 K/min

where A is a constant and equals 1.0516, $E_a(x)$ the local activation energy when the crystallization fraction is x, C_2 a constant, and $T(x)$ the temperature corresponding to x. The $E_a(x)$ values for different crystallization fractions can be calculated from the slope of $\ln\beta$ vs. $1/T$ plot. As shown in Fig. 7, the local activation energy tends to decrease with increasing the crystallization volume fraction. It suggests that the crystallization will become easier as the crystallization process develops. The average activation energy in the entire crystallization process is 252 ± 13 kJ/mol for the present alloy, slightly less than the effective activation energy obtained by Kissinger and Ozawa equations. This difference may be caused by the exothermic reaction during the crystallization process.

The local Avrami exponent of crystallization is helpful for understanding the mechanisms of nucleation and growth of new crystalline grains during phase transition, which can be obtained by the following Johnson–Mehl–Avrami equation [28–33]:

$$x = 1 - e^{-(kt)^n} \tag{4}$$

where x is the crystallization volume fraction at time t, n is the Avrami exponent related to the nucleation and growth and k is the reaction rate constant related to absolute temperature described by Arrhenius equation:

$$k = k_0 e^{\frac{-E_a}{RT}}, \tag{5}$$

where k_0 is a constant, E_a the effective activation energy of crystallization, R the gas constant, and T the absolute temperature. In terms of the Johnson–Mehl–Avrami equation, n can be yielded from the slope of $\ln(-\ln(1-x))$ versus $1000/T$ plot. It should be noted that this equation is only suitable for isothermal crystallization process. If a non-isothermal crystallization is considered, the following equation would be applicable [34],

$$n(x) = \frac{-R\partial \ln[-\ln(1-x)]}{E_a(x)\partial(1/T)} \tag{6}$$

by which the local Avrami exponent $n(x)$ can be obtained according to the local activation energy $E_a(x)$. Figure 8 shows the local Avrami exponent as a function of crystallization volume fraction at the heating rate of 30 K/min. It can be seen that the Avrami exponent decreased as temperature increased.

Based on the physical nature of Avrami exponent, Ranganathan and Heimendahl proposed a relationship to describe the nucleation and growth of crystalline grains, that is [35]

$$n = a + bc \tag{7}$$

where a is the nucleation index, in which $a = 0$ means zero nucleation rate, $0 < a < 1$ means that nucleation rate decreases with time and $a = 1$ means that nucleation rate increases with time; b is the dimension of growth ranged from 1 to 3, in which $b = 1$, 2, and 3 mean one-, two- and three-dimensional growth, respectively; and c is the growth index, in which $c = 1$ means interface-controlled growth and $c = 0.5$ means diffusion-controlled growth. For the present $Al_{75}Ni_{10}Ti_{10}Zr_5$ amorphous alloy, the Avrami

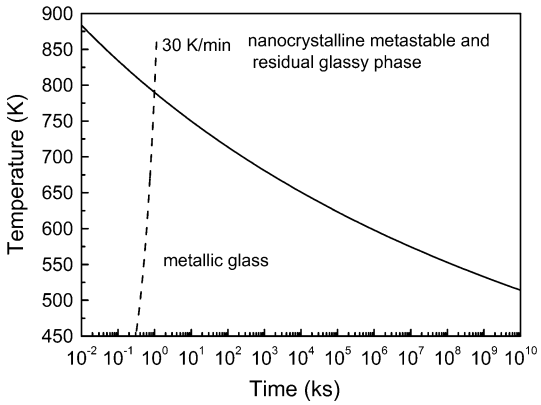

Fig. 9 Continuous heating transformation diagram of the $Al_{75}Ni_{10}Ti_{10}Zr_5$ amorphous alloy, where the *dashed vertical line* represents a heating rate of 30 K/min

exponent gradually decreased from 4.0 to about 2.0 as the crystallization proceeded, indicating that the dominant growth is two- and three-dimensional growth controlled by diffusion, as shown in Fig. 8.

It can been seen from the above DSC results that both T_x^{onset} and ΔT_x varies with heating rate, and thus these two parameters are inadequate in evaluating the thermal stability of amorphous alloys. Recently, some researchers conducted studies to evaluate the long-term thermal stability of amorphous alloys through the Kissinger equation [36, 37]. Figure 9 shows the continuous heating transformation diagram of the present $Al_{75}Ni_{10}Ti_{10}Zr_5$ amorphous alloy constructed by the Kissinger equation. The dashed line in the Fig. 9 indicates a situation at the heating rate of 30 K/min. It is found that the onset crystallization temperatures remain almost unchanged during an extremely long period, and if the onset crystallization temperature decreases to a relatively low temperature, for instance 500 K, the time needed is longer than 100,000 years. Thus, the amorphous alloy will devitrify even at room temperature at sufficiently large time scale, indicating the stability of the present $Al_{75}Ni_{10}Ti_{10}Zr_5$ alloy could be thought to be high enough.

Conclusions

The formation and crystallization behavior of a mechanical alloyed $Al_{75}Ni_{10}Ti_{10}Zr_5$ amorphous alloy was characterized by X-ray diffraction, transmission electron microscopy, and differential scanning calorimetry. The effective activation energy for the crystallization was determined by both the Kissinger and Ozawa equations. It is found that the average local activation energy is 252 ± 13 kJ/mol, and the Avrami exponent lies between 2.0 and 4.0 that correspond to the crystallization volume fractions ranged from 0.3 to 0.9. This demonstrates that the crystallization mechanism of the present alloy is two- and three-dimensional nucleation and growth controlled by diffusion. The long-term thermal stability was evaluated by a continuous transformation diagram obtained from the extension of Kissinger analysis.

Acknowledgements This work is supported by the National Basic Research Program of China in the no. 2006CB601201, the National Natural Science Foundation of China in the no. 50871107.

References

1. Greer AL (1995) Science 267:1947
2. Guo FQ, Poon SJ, Shiflet GJ (2000) Mater Sci Forum 331–337:31
3. He Y, Poon SJ, Shiflet GJ (1988) Science 241:1640
4. Amini R, Hadianfard MJ, Salahinejad E, Marasi M, Sritharan T (2009) J Mater Sci 44:136. doi:10.1007/s10853-008-3117-9
5. Prashanth KG, Scudino S, Surreddi KB, Sakaliyska M, Murty BS, Eckert J (2009) Mater Sci Eng A 513–514:279
6. Lin HM, Lin YW, Lee PY (2008) J Mater Sci 43:3118. doi:10.1007/s10853-008-2504-6
7. Yang DK, Wen CE, Han FS, Yang YJ (2006) J Non-Cryst Solids 352:3244
8. Wang Y, Chen XX, Geng HR, Yang ZX (2009) J Alloys Compd 474:152
9. Bae DH, Lee MH, Kim DH, Sordelet DJ (2003) Appl Phys Lett 83:2312
10. Lee MH, Bae DH, Kim DH, Sordelet DJ (2003) J Mater Res 18:2101
11. Zhu J, Clavaguera-Mora MT, Clavaguera N (1997) Appl Phys Lett 70:1709
12. Hay CC, Kim CP, Johnson WL (2000) Phys Rev Lett 84:2901
13. Inoue A (1998) Prog Mater Sci 43:365
14. Gloriant T, Greer AL (1998) Nanostruct Mater 10:389
15. Zhong ZC, Jiang XY, Greer AL (1997) Mater Sci Eng A 226–228:531
16. Suryanarayana C (2001) Prog Mater Sci 46:1
17. Samanta A, Manna I, Chattopadhyay PP (2007) Mater Sci Eng A 464:306
18. Yue YZ (2008) J Non-Cryst Solids 354:1112
19. Kissinger HE (1957) Anal Chem 29:1702
20. Ozawa T (1970) J Therm Anal 2:301
21. Kim DH, Kim WT, Kim DH (2004) Mater Sci Eng A 385:44
22. Gogebakan M, Warren PJ, Cantor B (1997) Mater Sci Eng A 226–228:168
23. Prashanth KG, Scudino S, Murty BS, Eckert J (2009) J Alloys Compd 477:171
24. Surreddi KB, Scudino S, Sakaliyska M, Prashanth KG, Sordelet DJ, Eckert J (2010) J Alloys Compd 491:137
25. Kissinger HE (1956) J Res Natl Bur Stand 57:217
26. Ligero RA, Vázquez J, Villares P, Jiménez-Garay R (1989) Mater Lett 8:6
27. Flynn JH (1983) J Therm Anal 27:95
28. Avrami M (1939) J Chem Phys 7:1103
29. Kaloshkin SD, Tomilin IA (1996) Thermochim Acta 280–281:303
30. Hampel G, Pundt A, Hesse J (1992) J Phys Condens Matter 4:3195
31. Barandiarán JM, Tellería I, Garitaonandía JS, Davies HA (2003) J Non-Cryst Solids 329:57

32. Cserei A, Jiang J, Aubertin F, Gonser U (1994) J Mater Sci 29:1213. doi:10.1007/BF00975066
33. Christian JW (2002) The theory of transformations in metals and alloys—parts I and II, 3rd edn. Pergamon, Oxford, UK
34. Lu W, Yan B, Hang WH (2005) J Non-Cryst Solids 351:3320
35. Ranganathan S, Heimendahl MV (1981) J Mater Sci 16:2401. doi:10.1007/BF01113575
36. Louzguine DV, Inoue A (2002) Scr Mater 47:887
37. Louzguine DV, Inoue A (2002) Appl Phys Lett 81:2561